Stress reduction in a-C:H coatings through the addition of nitrogen to the feed gas

F. Rabbani[a,*], R. Escobar Galindo[b], W.M. Arnoldbik[c], S. van der Zwaag[d], A. van Veen[b,✠], H. Schut[b]

[a] *Department of Materials Science, Delft University of Technology, Rotterdamsweg. 137, 2628 AL Delft, The Netherlands*
[b] *Interfaculty Reactor Institute, Delft University of Technology, Mekelweg. 15, 2629 JB Delft, The Netherlands*
[c] *Surfaces, Interfaces and Devices, Debye Institute, Utrecht University, P.O. Box 80.000, 3508 TA, Utrecht, The Netherlands*
[d] *Faculty of Aerospace Engineering, Delft University of Technology, Kluyverweg. 1, 2629 HS Delft, The Netherlands*

Abstract

Intrinsic stress in amorphous hydrogenated carbon (a-C:H) coatings was reduced through addition of 10–20 sccm N_2 to the feed gas. The compressive stresses observed in this study were in the range −0.91 to −1.6 GPa. Approximately 2–3 at.% nitrogen was incorporated into the coatings as determined using elastic recoil detection (ERD). Raman spectroscopy shows that the G peak of samples made with nitrogen is shifted to higher wave numbers, and that there is a more pronounced 'shoulder' at the D peak position. It is hypothesized that nitrogen addition to the feed gas at a flow rate of 20 sccm enhances the formation of aromatic rings associated with the D peak. The stress reduction noted for nitrogen addition at 10 sccm was contributed to a reduction in the mean coordination number of the network. Positron beam analysis (PBA) was used to show that in a high temperature deposition the interface of the nitrogen-containing coating has more open space. This phenomenon can contribute to a reduction of the compressive stress by reducing the interfacial stress. Annealing tests were performed to monitor this open volume using Raman and PBA analysis.

Keywords: Amorphous hydrogenated carbon; Vibrational properties characterization; Defect characterization

1. Introduction

Some of the attractive properties of amorphous hydrogenated carbon (a-C:H) coatings are their low coefficient of friction, good wear rate, chemical inertness and low surface energy. A problem in the manufacture of these coatings is their high intrinsic stress, which results in coating failure. In this research the adhesion of a-C:H coatings onto steel and Si substrates was noted to improve with the addition of nitrogen to the gas plasma. Other researchers have also reported better adhesion and/or a reduction of the coating stress with nitrogen incorporation [1–6]. The following systematic study was undertaken to investigate the reduction in the intrinsic stress of a-C:H coatings deposited onto Si wafers with nitrogen in the gas feed at 10 and 20 sccm flow rates. These a-C:H coatings were produced by a non-conventional process: the decomposition of a reactive plasma was achieved in a PVD chamber by applying a DC-bias voltage to the substrate table while gases were introduced into the evacuated chamber at set flow rates. The gas composition was varied from pure CH_4, CH_4+Ar, to CH_4+H_2, in each case a sample was also deposited with nitrogen in the gas feed. It was seen that addition of 10 sccm nitrogen had some effect but not as much as 20 sccm in reducing the intrinsic stress. This stress was in all the cases compressive and in the range of stresses reported for these coatings in the literature [7]. As the deposition temperature is also a variable that affects film growth, two samples were made at 300 °C to isolate the effect of nitrogen addition. In all cases, the compressive stress in the coatings decreased with the addition of nitrogen. In depo-

* Corresponding author. Tel.: +31-1527-89518; fax: +31-1527-86730.
E-mail address: f.rabbani@tnw.tudelft.nl (F. Rabbani).
✠ Deceased 3 January 2004.

sitions where heating was not applied to the process, the elastic modulus was also reduced with nitrogen addition at 20 sccm. In the case of the high temperature depositions, the reduction in the elastic modulus was noted for both samples.

The stress in the coatings was determined through radius of curvature measurements made on the Si substrate before and after deposition. The mechanical properties of the coatings such as the elastic modulus and hardness were measured using nano-indentation testing. Elastic recoil detection yielded information on the composition of the films and show that 2–3 at.% nitrogen is incorporated. This research uses positron beam analysis (PBA) and Raman spectroscopy as complementary techniques to study a-C:H coatings. As hydrogen present at voids essentially masks these defects for PBA detection [8], a series of annealing tests were carried out to 'isolate' open space after out diffusion of hydrogen. Unique to this study is the finding that the D peak becomes more pronounced, significant of augmentation in size or number of aromatic ring structures.

2. Experimental

A Hauzer PVD machine was used to generate a reactive glow made from the decomposition of a range of gas mixtures with and without N_2, where CH_4 was the carbon containing gas. Even though a PVD chamber was used the process is unique in that target sputtering was not employed. The PVD chamber was first pumped down to a vacuum of approximately 10^{-4} Pa. Prior to the coating procedure an etch step was included using Ar gas to remove the surface oxide layer on the Si substrate. The plasma was generated through the application of a bias voltage of 550 V-DC to a rotating substrate table, while the gases were introduced at specific flow rates high enough to generate a glow discharge. The coatings were deposited onto Si (100) single crystal substrates, for a deposition time of 1 h. During deposition the process temperature rises gradually to some equilibrium value less than 300 °C due to the heat generated by ion bombardment. Two samples were made with temperature regulation, i.e. the deposition was started at 300 °C and this temperature was maintained during the test by applying external heating not generated by the plasma itself. The annealing tests were conducted at 150, 300, 400, 500 and 600 °C in a vacuum of 10^{-5} Pa for 30-min intervals. PBA and Raman spectroscopy were used to monitor the changes that occurred in the coatings between each annealing experiment.

2.1. Stress measurements

Stress measurements were made by determining the radius of curvature of the Si wafer before and after deposition, using a bending laser beam method. Details of the experimental set-up can be found in Ref. [9]. The stress was calculated using a modified Stoney equation [10]:

$$\sigma = [E_{Si}/(1-\nu_{Si})](t_{Si}^2/6t_c)(1/R_c - 1/R_{Si}) \quad (1)$$

where σ is the stress in the coating, E_{Si} the elastic modulus of the Si wafer, ν_{Si} the Possion's ratio of the Si wafer, t_{Si} the thickness of the Si wafer, t_c the thickness of the coating (determined by weight gain measurements and assuming a density for the a-C:H coating of $2.0\times10^{+3}$ kg m^{-3}). R_{Si} is the radius of curvature of the Si substrate before deposition and R_c the radius of curvature after deposition.

2.2. Nano-indentation testing

The elastic modulus and hardness of the coatings were measured with a Hysitron TriboScope® nanomechanical test instrument equipped with a Berkovich diamond tip. The software calculates the elastic modulus by taking the linear portion of the unloading curve. Simultaneously, hardness is calculated by subtracting the elastic displacement from the load-displacement data [11].

2.3. Raman

A Renishaw Raman microscope system 2000, using the 514.5 nm line of an Ar ion laser was used for the spectroscopy analysis. The measurements were made at a laser power setting of 2 mW, and the system was calibrated with a Si specimen. Grams 32 software was applied to subtract a linear background from the spectra and to fit two curves of a mix Gaussian–Lorentzian function in the region 1000–1750 cm^{-1}. All the fit parameters such as linewidth, positions and areas were allowed to vary. The G peak is due to the relative stretching motion of sp^2 carbon atoms in rings or chains; and the D peak is due to the breathing modes of aromatic rings [12]. The I_d/I_g ratio was determined based on peak areas.

2.4. PBA

The PBA experiments were performed with the Delft Variable Energy Positron beam (VEP) [13]. The positrons were injected in the samples with energies tuned between 100 eV and 30 keV. The maximum implantation energy corresponds to a typical mean implantation depth of ~4 μm in materials with a density of ~3 g cm^{-3}. All experiments were carried out at room temperature under a vacuum of approximately 10^{-6} Pa. PBA results are described in terms of two parameters describing the Doppler broadening of the 511 keV annihilation photo-peak. The *S* parameter indicates the fraction of positrons that annihilate with low momentum electrons (small Doppler broadening) such as valence or conduction electrons. This parameter is related to the open volume defects present in the sample such as vacancy clusters and/or interfaces with misfit. *S* increases as the

Table 1
Sample references corresponding with set process variables that produce a-C:H coatings with the given coating thickness (t), E and H values, and compressive stress

Sample	Pressure (Pa)	T range (°C)	t (nm)	E (GPa)	H (GPa)	Stress (GPa)
100 sccm CH_4 N2	9.6	50–145	582	125.5±2.3	14.3±0.6	1.4
100 sccm CH_4+20 sccm N_2 Ar	12	53–226	441	115.3±2.6	14.4±0.6	1.1
50 sccm CH_4+30 sccm Ar ArN2	7.8	103–180	345	132.1±2.9	15.5±0.8	1.6
50 sccm CH_4+30 sccm Ar+10 sccm N_2 Ar2N2	7.8	105–134	365	121.1±3.2	15.3±1.0	1.3
50 sccm CH_4+30 sccm Ar+20 sccm N_2 H2	8.3	108–180	335	109.5±4.3	13.0±0.9	0.91
50 sccm CH_4+50 sccm H_2 H2N2	7.7	300–300	182	106.4±5.1	9.7±2.2	1.5
50 sccm CH_4+50 sccm H_2+20 sccm N_2	8.3	300–300	122	109.8±4.4	9.7±3.0	1.2

open-volume defects in a material increase, and larger values of S indicate that the material has more open-volume defects [8]. The W parameter indicates the fraction of positrons that annihilate with high momentum electrons (core electrons) and thus cause larger Doppler broadening. This parameter is related to the chemical environment where the annihilation takes place. Both parameters can be combined in $S-W$ maps where the different annihilation sites can be distinguished. The data were analyzed with the VEPFIT program [14]. The S and W parameters of the Si substrate were used to normalize the data (as these values are identical for all samples, it allows for comparisons to be made between coatings and among annealing tests). Although positron annihilation sites can occur at the surface, in the bulk of the coating, at the coating-substrate interface, and in the silicon substrate, only the coating and the interface values are of interest in this study. These annihilation sites can be distinguished by selecting the positron implantation energy.

2.5. ERD

The elastic recoil detection [15] (ERD) measurements were carried out employing 50 MeV Cu^{8+} ions produced by the 6 MV EN Tandem van de Graaff accelerator at Utrecht University. These ions can profile all elements from hydrogen to silicon to a depth of a few hundred nanometer in one single measurement. However, in the case of large hydrogen concentrations, hydrogen tends to desorb from the layers under heavy ion irradiation [16]. Therefore, the hydrogen concentration was determined in a separate, short, measurement using a large opening angle. During this measurement the hydrogen content in the film was monitored as a function of ion dose, and this curve is extrapolated to its initial value to determine the hydrogen content. For the hydrogen measurements a solid-state detector at an angle of φ=30° with the beam direction was used. A 29 μm Mylar absorber foil prevents particles other than hydrogen from entering the detector. The incidence angle between the ion beam and the sample surface was set to 20°. Subsequently, the other elements were measured under the same geometry, using a ΔE-E ionization chamber with a Frisch grid as the particle detector. No Ar was detected in the coatings using energy dispersive X-ray spectroscopy analysis.

3. Results

3.1. Nano-indentation testing and radius of curvature measurements

Table 1 summarizes the gas compositions and flow rates that were used to generate the plasma, with the corresponding values of elastic modulus (E), hardness (H), coating thickness (t) and compressive stress of the resultant coatings. The samples were given a code symbolizing the differences in the gas plasmas: R, N2, Ar, ArN2, Ar2N2, H2, H2N2 (where R is the reference plasma consisting of CH_4 gas only). Nano-indentation testing was used to arrive at the E and H values, and as described in the experimental section, stress in the coatings was determined by the radius of curvature method.

As the average particle energy of the impinging ions or neutrals is directly proportional to the term $V_B/P^{1/2}$ [17], the development of compressive stress is associated with the gas pressure (P) and the bias voltage applied (V_B). In this study, V_B was kept constant and P was varied between 7.7 and 12 Pa, however, no relationship between these variables and the stress in the film was observed. Different gas compositions produce coatings with different stress levels, and the only trend in stress reduction was related to the addition of nitrogen. Fig. 1 shows that in all cases, the measured stress in the coatings is lower with nitrogen

addition, with more pronounced effects occurring at 20 sccm flow rate. In the case of depositions made at temperatures lower than 300 °C, there is a concurrent reduction in the elastic modulus with nitrogen addition, but a clear trend does not emerge for a reduction in the hardness values. At high process temperature, i.e. 300 °C, there is little difference between the *E* and *H* values of the nitrogen containing coatings and the control, however, compared to the low temperature depositions these variables are greatly reduced. The stress reduction associated with nitrogen inclusion is also evident for this test.

3.2. ERD

The compositional variation of the a-C:H coatings with and without nitrogen inclusion has been determined with ERD and the results are summarized in Table 2. It can be seen that all the samples made with nitrogen in the plasma are doped, including the sample made at a nitrogen flow rate of 10 sccm. The nitrogen incorporation varies approximately between 2 and 3 at.%, and the relationship between nitrogen content and stress reduction is displayed in Fig. 2. There is a 5–8 at.% decrease in hydrogen content for coatings containing nitrogen as compared with the control counterparts; the greatest effect is observed for the depositions at lower temperatures. ERD shows that after annealing to 600 °C, the hydrogen content has decreased by 50–58% of its original value.

Table 2
Compositional variation of the samples as measured with ERD including the nitrogen to carbon ratio (N/C)

Sample	H (at.%)	N (at.%)	N/C
R	27	0.07	0.001
N2 (20 sccm N_2)	19	2.1	0.026
Ar	27	0.18	0.002
ArN2 (10 sccm N_2)	21	2.2	0.029
Ar2N2 (20 sccm N_2)	22	2.9	0.038
H2	31	0.42	0.006
H2N2 (20 sccm N_2)	26	2.9	0.041
H2 after final anneal	12	–	–
H2N2 (20 sccm N_2) After final anneal	13	–	–

3.3. Raman spectroscopy of as deposited coatings

The Raman spectra of the as deposited coatings, (not including the high temperature deposition), are shown in Fig. 3. There is a more distinct 'shoulder' in the spectra for samples made with 20 sccm nitrogen. These results are summarized in Table 3 for all coatings and include the G and D peak positions, the G and D peak line widths (measured at full width half maximum (FWHM)), I_d/I_g ratios, and approximate sp^3 content. In amorphous carbons, the development of a D peak indicates ordering, and I_d/I_g is proportional to the number and clustering of rings [12]. The intensity maximum of the D peak relative to the G peak is directly related to the existence of six-fold aromatic rings, while a broadening of the D peak can be correlated with ring orders other than six [12].

The width of the G peak is proportional to bond-angle disorder at sp^2 sites [12]. Fig. 4 is a plot of the G peak linewidth as a function of the measured stress for coatings made without nitrogen, and with nitrogen at a flow rate of 20 sccm in the gas feed. It can be seen from this figure and the data in Table 3 that the line width of the G peak decreases when nitrogen is included at a flow rate of 20 sccm relative to the gas composition without nitrogen. This is indicative of less bond angle disorder at sp^2 sites which in turn means that the system is less constrained and, therefore under less stress. Schwan et al. [18] show that as the intrinsic stress increases

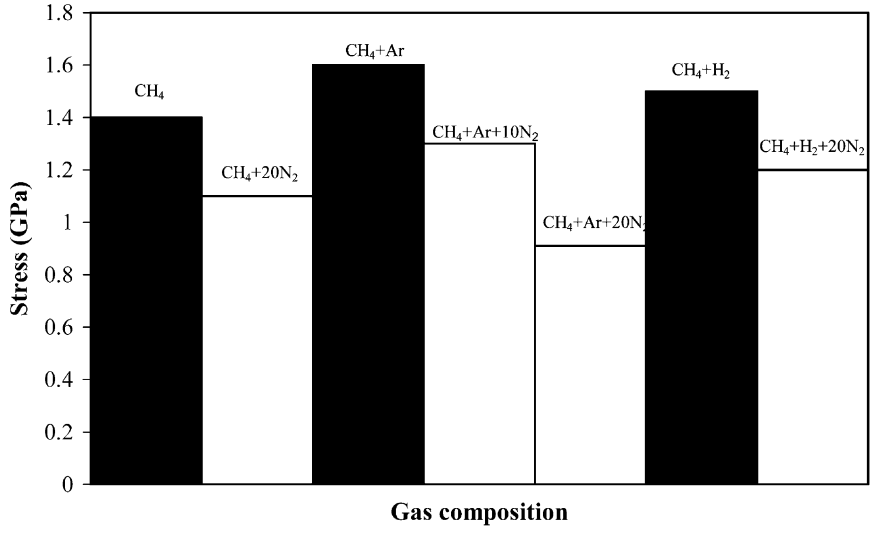

Fig. 1. Bar graphs showing the reduction in the compressive stress with the addition of nitrogen for different sets of gas compositions used to generate the plasma.

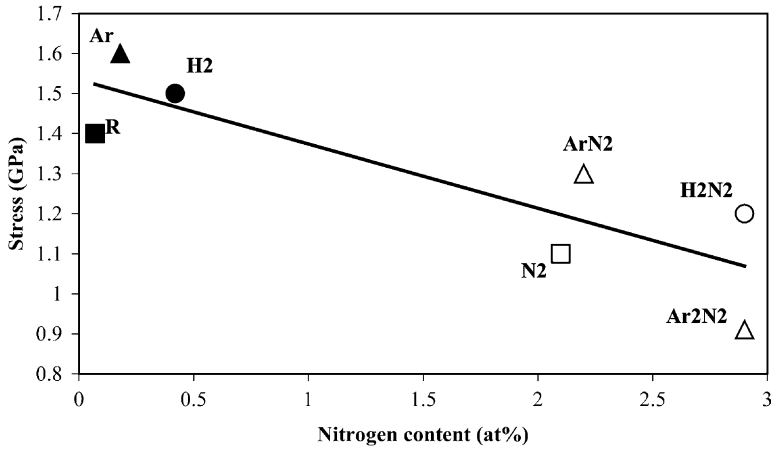

Fig. 2. Relationship between the compressive stresses measured for the a-C:H coatings and their nitrogen content. (Unfilled symbols correspond to coatings made with nitrogen in the gas plasma).

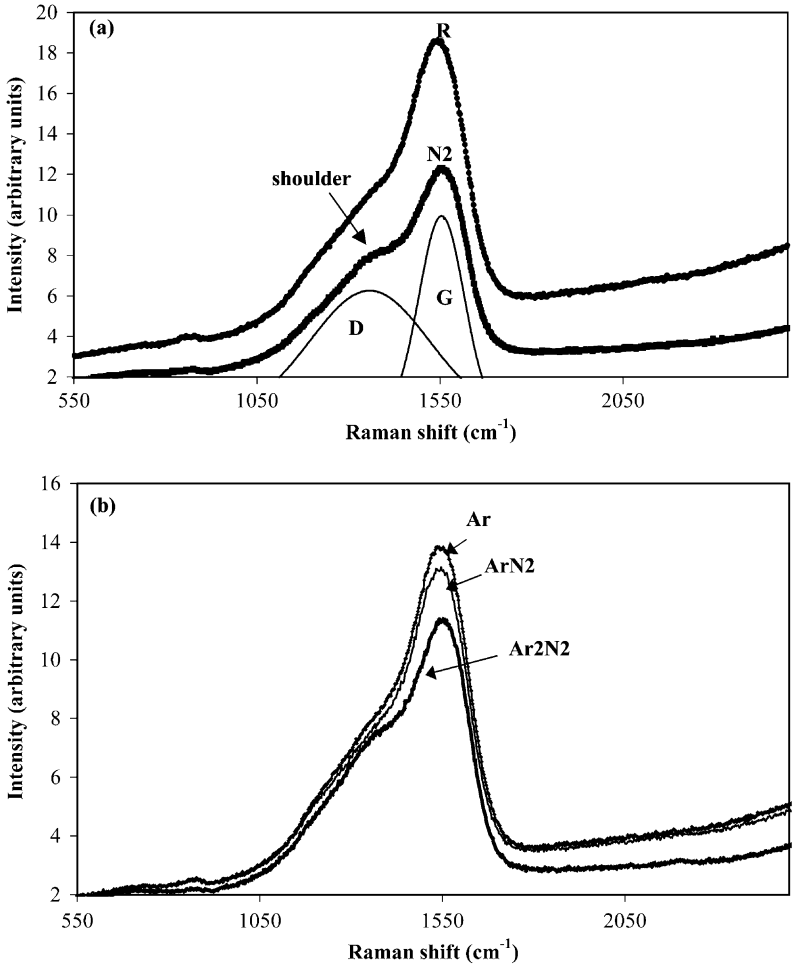

Fig. 3. Raman spectra for as deposited coatings with and without nitrogen addition. (a) Raman spectra for coatings R and N_2 showing development of enhanced 'shoulder' with the addition of nitrogen, (schematic of the fitted D and G peaks have been included). (b) Samples Ar, ArN2 and Ar2N2 compose the series made with CH_4/Ar, with 10 and 20 sccm nitrogen inclusion-a broadening of the 'shoulder' only occurs with 20 sccm nitrogen addition.

Table 3
G and D peak position, line widths, I_d/I_g ratios, sp^3 fraction and cluster diameter (L_a) for a-C:H coatings made with and without N_2

Sample	Nitrogen flow (sccm)	G peak (cm^{-1})	Line width of G peak (cm^{-1})	D peak (cm^{-1})	Line width of D peak (cm^{-1})	I_d/I_g	Approximate sp^3 content (%) [12]	L_a (Å)
R	0	1552	154	1389	364	1.5	35	16.5
N2	20	1564	131	1407	399	3.0	25	23.3
Ar	0	1554	156	1396	380	1.7	30	17.6
ArN2	10	1553	155	1394	386	1.8	30	18.1
Ar2N2	20	1562	142	1404	382	2.5	25	21.3
H2	0	1566	142	1410	384	2.4	25	20.9
H2N2	20	1574	126	1412	374	3.1	25	23.7

the G peak line width increases; therefore coatings under lower intrinsic stress have a smaller G peak line width.

The variation in the D peak width between coatings made in a plasma containing nitrogen as compared with its corresponding counterpart containing no nitrogen was only significant for samples R and N2, (the differences among the other sets were too close to the error in the peak fit analysis to establish conclusive findings). The width of the D peak is greater for the coating deposited using a methane/nitrogen (N2) mixture as compared with the pure methane plasma (R), indicating that the coating contains a greater diversity of aromatic ring orders [12].

The data in Table 3 illustrate that with nitrogen addition the G peak shifts to higher wave numbers, and the I_d/I_g ratio increases. It has been shown using EELS spectroscopy that sp^2 bonding increases as a function of nitrogen content for films of a-C:H [19]. As it was not possible to do EELS spectroscopy in this study, an sp^3 fraction was approximated using the analysis of Robertson and Ferrari [12] based on the G peak position and the I_d/I_g ratio. They obtained a relationship between sp^3 content and these Raman parameters for as deposited a-C:H, by fitting a line to the experimentally obtained data of sp^2 content and optical gap [12]. In this study, this analysis was further extended to estimating an sp^3 content for the doped coatings since the nitrogen content in the films was too low to establish the presence of a CN phase, and any changes observed in the optical gap were attributed to variation in the sp^2 content. This estimate shows that the sp^3 content is lower for samples made with 20 sccm nitrogen. In addition, the high temperature deposition at 300 °C (H2) also has a lower sp^3 content or higher sp^2 content than control coatings made at lower temperatures.

The cluster diameter or in-plane correlation length of aromatic clusters, L_a, was calculated based on the following relation:

$$I_d/I_g = C'(\lambda)L_a^2 \quad (2)$$

Where C' (514 nm)=0.0055 ($Å^{-2}$) (Although this equation is used to arrive at L_a for coatings studied in this research, the comparison is comparative, i.e. the value for L_a is most likely overestimated as suggested by Schwan et al. [18]). The resulting L_a values are included in Table 3. The plot of L_a against the G peak position and G peak width is illustrated in Fig. 5. It can be seen that in general L_a is bigger (e.g. H2N2) and/or that there are more aromatic clusters (e.g. N2) with nitrogen inclusion, and as the value of L_a

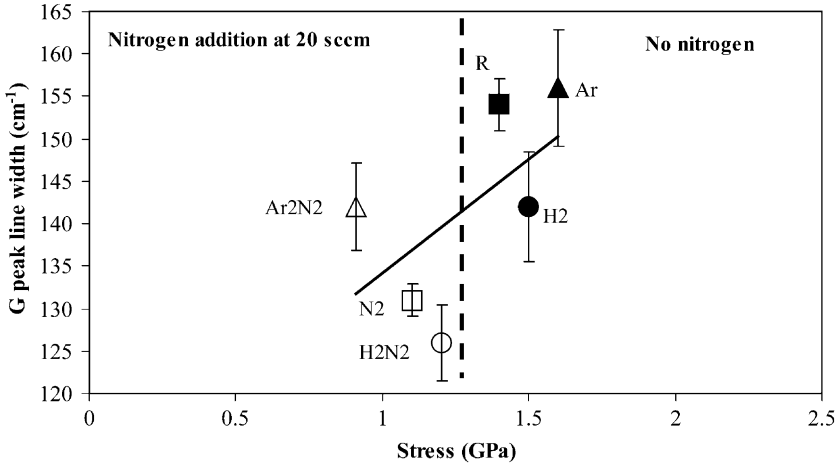

Fig. 4. Changes in G peak line width as a function of stress for coatings made with various plasma compositions with and without nitrogen addition at 20 sccm. (The dotted line was arbitrarily drawn to show the demarcation in stress level between coatings made with nitrogen and those made without nitrogen).

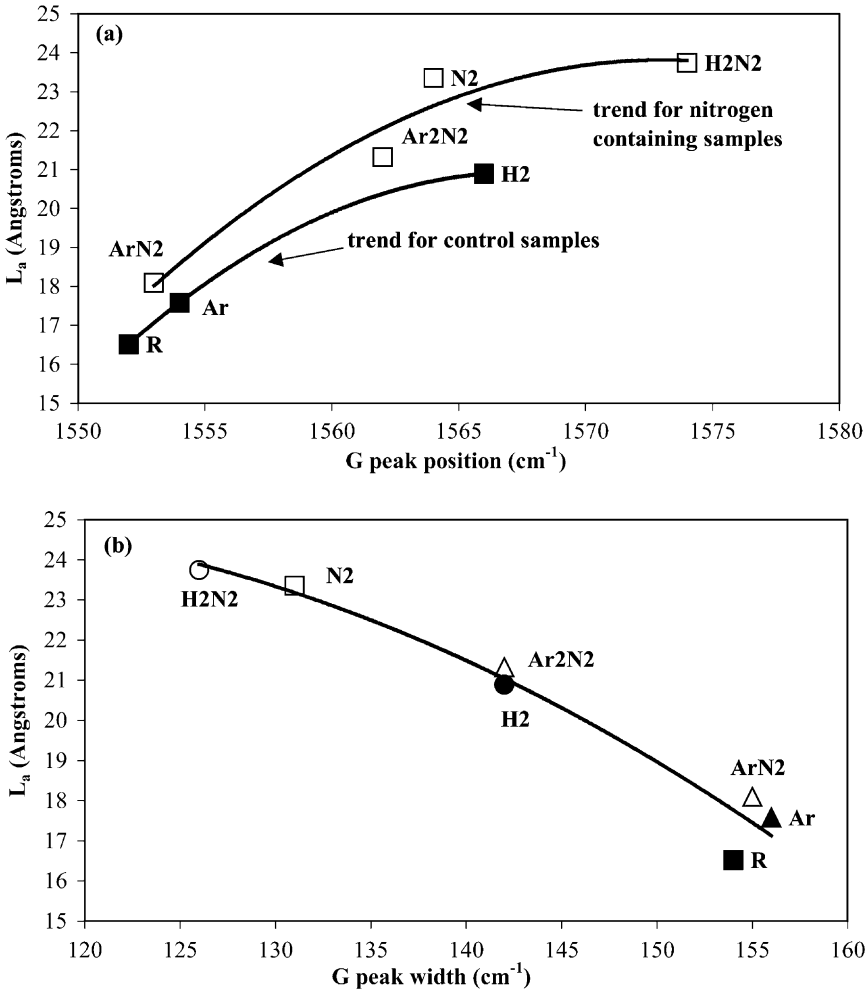

Fig. 5. Changes in the cluster size with nitrogen inclusion: (a) Shows variation of cluster size with G peak position for samples with and without nitrogen. (b) Illustrates that as the cluster size increases, the G peak width decreases. (Unfilled symbols represent samples made with nitrogen in the plasma.)

increases the G peak position moves to higher wave numbers and the width decreases. The latter observation, i.e. decrease in width of the G peak, has been linked with stress reduction [18]. As noted before from the variation in the D peak width, sample N2 has a larger diversity of aromatic ring orders so the larger value of L_a in this case is attributed to an increase in number of clusters. The larger value of L_a for H2N2 corresponds with an increase in the six-membered aromatic cluster size as the D peak width has not increased and the G peak has shifted to higher wave numbers.

3.4. Annealing study: using Raman spectroscopy and positron beam analysis

3.4.1. Raman spectroscopy

Two samples were made at the regulated and elevated temperature of 300 °C, to isolate the effect of nitrogen on stress development at high temperatures. That is, to observe if a high temperature deposition, which may be conducive to the generation of a higher thermal stress component, is influenced by the presence of nitrogen in the gas plasma. As seen in Table 1, the stress is reduced with nitrogen inclusion and the Raman spectra show that although both samples have a 'shoulder', the sample manufactured with 20 sccm nitrogen has a more pronounced 'shoulder'. Fig. 6 displays the Raman spectra of the as deposited coatings and their final evolution after annealing to 600 °C. As mentioned before, the annealing experiments were performed to identify open volume in the samples. The evolution of the G and D peak positions, and the changes in their line widths, as a function of annealing temperature is listed in Table 4.

The graphitization process is underway at 300 °C for the nitrogen-containing sample, H2N2, as the G peak position is at 1580 cm^{-1}. However, for the coating made without nitrogen, H2, 300 °C marks the start of the process as seen by the movement of the G peak to higher wave numbers. This behavior is linked with the fact that the as deposited coating with nitrogen in the gas plasma has a G peak that is shifted to higher wave numbers, 1574 cm^{-1} as compared

with the G peak of the methane/hydrogen mixture which is at 1566 cm^{-1}. The transformation to a graphitic structure with annealing has been linked to the release of bounded hydrogen between 400 and 600 °C [20]. In this temperature range sp^3 carbon bonds are transformed to sp^2 bonds [21]. As seen before, the width of the G peak is less for the nitrogen containing samples—therefore, less bond angle disorder at sp^2 sites. A general trend of decreasing bond angle disorder with increasing annealing temperature is recorded for both samples.

There is a shift of the D peak position with annealing temperature to lower wavelengths. The wavelengths 1353 and 1598 cm^{-1} are associated with small crystallites of graphite, and in the proximity of 1353 cm^{-1} it can be concluded that the crystallites formed are three-fold coordinated [22]. A fine-grained polycrystalline structure emerges as the coating becomes more graphitic in nature, i.e. the clusters will lose their molecular like properties [19]. The changes in the D peak width with annealing temperature shows that ordered clusters of six-membered rings (crystallites) dominate as the sample is heated. These transformations can also be seen in the PBA data.

Table 4
Shift of the G and D peaks and changes in peak widths as a function of annealing temperature

T (°C)	G peak position (cm^{-1})		G peak line width (cm^{-1})		D peak position (cm^{-1})		D peak line width (cm^{-1})	
	H2N2	H2	H2N2	H2	H2N2	H2	H2N2	H2
As deposited	1574	1566	126	142	1412	1410	374	384
150	1573	1565	123	142	1419	1409	406	381
300	1580	1571	115	131	1411	1403	365	375
400	1580	1576	109	120	1401	1405	352	366
500	1587	1590	103	103	1372	1375	333	310
600	1585	1585	107	101	1355	1349	316	314

3.4.2. PBA

The positron beam analysis data (Table 5) show that the open volume, as seen in the value of the *S* parameter is greater at the interface for both coatings as compared with

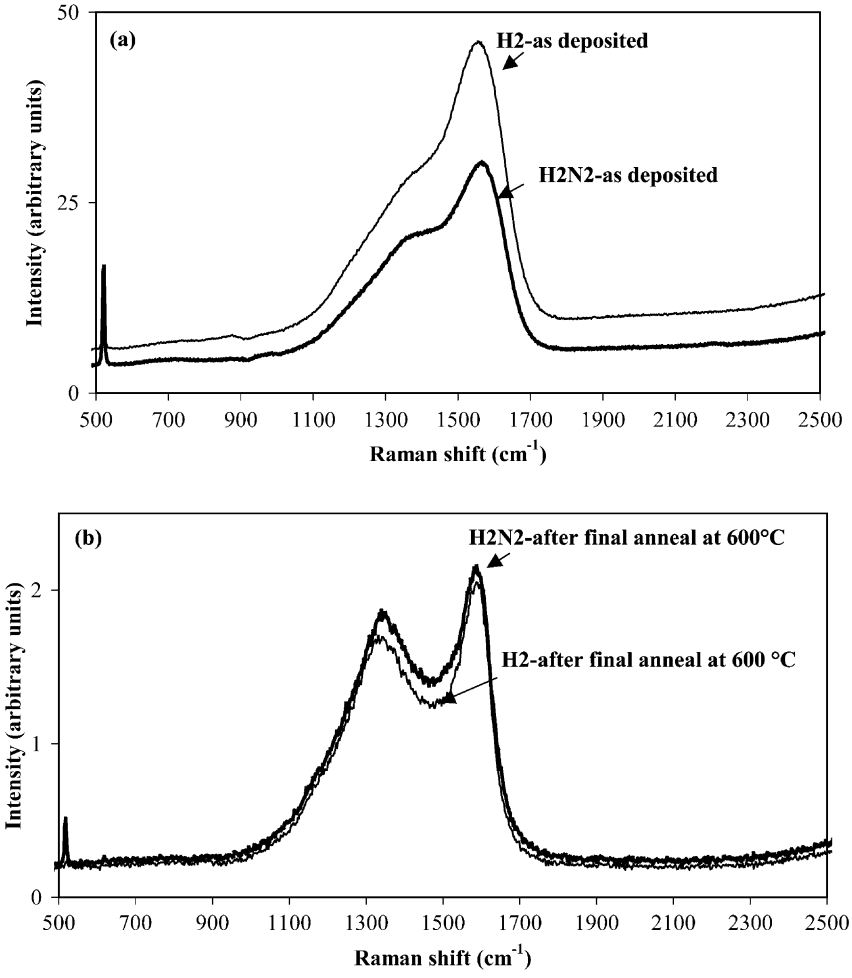

Fig. 6. Raman spectra for the high temperature depositions: (a) As deposited a-C:H films (H2N2 contains nitrogen); (b) Shows the final evolution of the Raman spectra after successive annealing procedures to 600 °C.

Table 5
VEPFIT results of samples studied at room temperature and after annealing to 600 °C (S_{Si}=1, W_{Si}=1). (The errors are $\Delta S \sim 0.002$ and $\Delta W \sim 0.03$)

Sample	Before annealing				After annealing			
	S_{coat}	W_{coat}	S_{interf}	W_{interf}	S_{coat}	W_{coat}	S_{delam}	W_{delam}
H2N2	0.932	1.40	0.964	1.33	0.929	1.48	0.906	1.68
H2	0.931	1.30	0.946	1.43	0.919	1.54	0.907	1.67

the bulk. The *W* parameter is also significantly different at the interface suggesting the existence of a mixed layer, which is created during the sub-plantation of the ions during deposition. The changes in the *W* parameter within the coating show that the chemical environment is changing with annealing. Both the *S* and *W* parameters have altered after the final anneal: the open volume has decreased, and the value of the *W* parameter has increased. The change in the *W* parameter of the coating for H2, (the sample made without nitrogen), is significantly greater than H2N2. At 600 °C PBA shows that there is 'delamination' of both coatings as the *S* and *W* parameters take on the value of the surface.

Fig. 7 shows the changes in the *S* and *W* parameters with annealing, and it becomes obvious that there are vacancy defects at the interface (Fig. 7a) of the nitrogen-containing sample (H2N2) since the *S* parameter is high and the *W* parameter low [23]. During the annealing procedure to 400 °C, the *S* parameter increases. This rise in the value of the *S* parameter can be seen more clearly in Fig. 8a, coincides with removal of physisorbed hydrogen [8]. However, at approximately 500 °C the gas released during the annealing is not only the release of 'unbound' hydrogen, but also the H bounded at tetrahedral sites to carbon, then there is a need for internal restructuring of the 'lattice', hence the decrease in the value of *S* at the interface. The chemical environment within the coatings, and at their interface, change with temperature as can be noted in the variation of the *W* parameter (Fig. 8b). Also evident in the plot of Fig. 8a is that the *S* parameter of the nitrogen containing coating, H2N2, is generally larger than that of the reference sample indicating that overall this coating has more open volume which is characteristic of a doped layer.

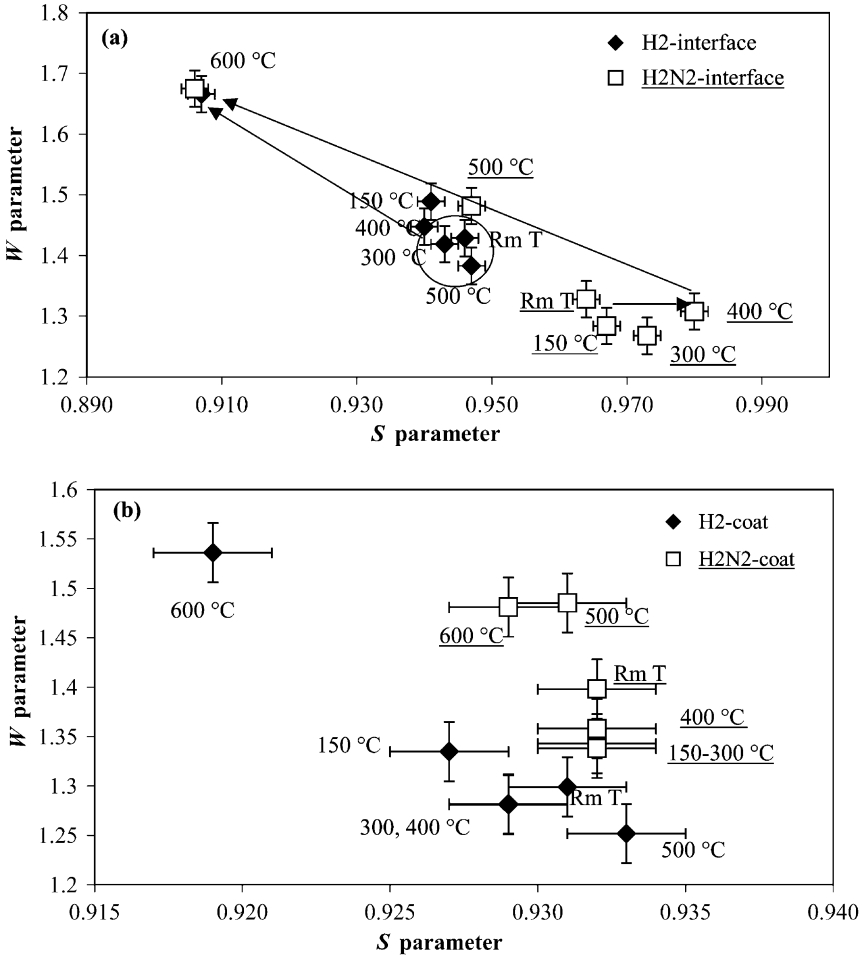

Fig. 7. *S*–*W* maps for the coatings made at high temperature, H2N2 and H2 showing the effects of annealing: (a) interface (b) coating. (Note: Fig. 7a and b are not to the same scale).

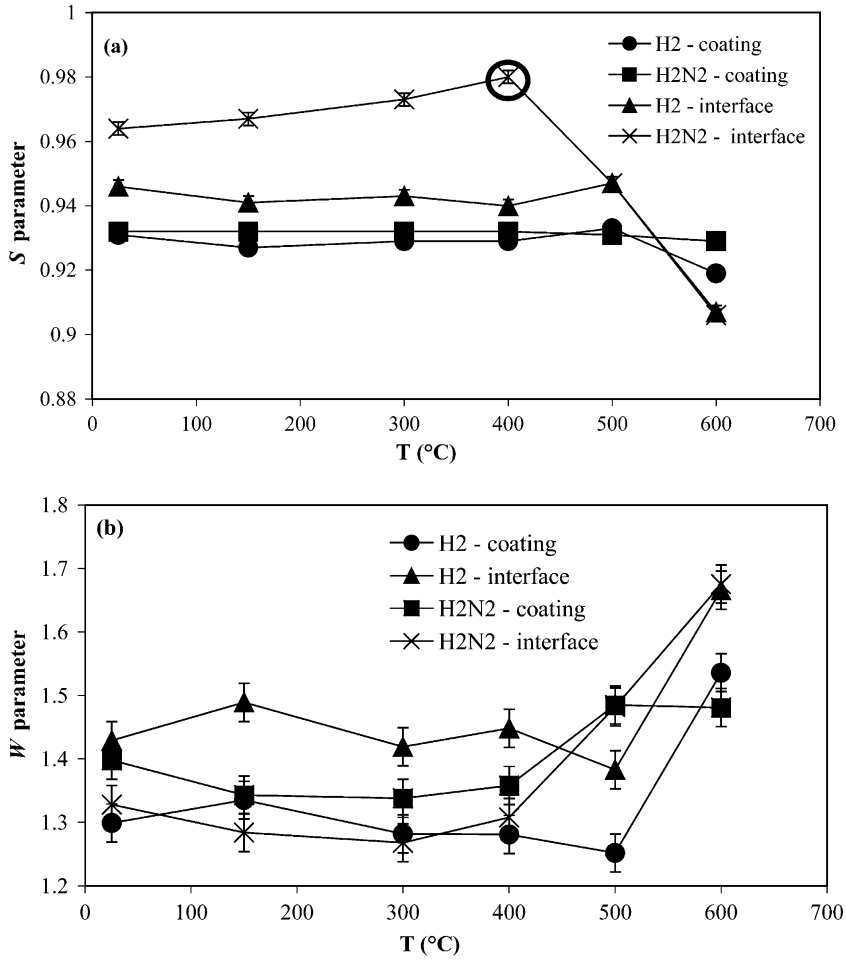

Fig. 8. The variation in the *S* and *W* parameters for the coatings and their interface as a function of annealing temperature (a) *S* parameter (b) *W* parameter.

4. Discussion

The measured stress is typically considered to be composed of a thermal and an intrinsic component. The thermal component arises from the mismatch between the thermal coefficients of expansion of the coating in relation to the substrate. In the case of Si substrates this contribution may be negligible [2] or tensile depending on the value of the coefficient of thermal expansion of the a-C:H coating. The coefficient of thermal expansion, α, for a-C:H was experimentally obtained by Lima et al. [24] as $3.0\pm0.20\times10^{-6}$ $^{\circ}C^{-1}$, while Wang et al. [25] derived α for DLC to be 7.0×10^{-6} $^{\circ}C^{-1}$. The value of this parameter for Si (100) crystal is quoted as 3.2×10^{-6} $^{\circ}C^{-1}$ [25], which means that the amorphous carbon coating either has the same value or a higher coefficient of thermal expansion. Based on this analysis it is concluded that for the purposes of this study the thermal component of the stress is not dominant in determining the overall stress. Furthermore, the thermal expansion coefficient for amorphous materials is dependent on the bond strain [26], therefore, materials with less bond strain such as the a-C(N):H will have a smaller coefficient of thermal expansion, closer to the value quoted for Si and better attachment.

How is intrinsic stress reduced with the addition of nitrogen? Certain phenomenological observations associated with the addition of nitrogen were noted in this study which are also corroborated by other researchers, such as:

1. G peak shifts to higher wave numbers [27,28]
2. Higher I_d/I_g ratios obtained with nitrogen addition [3,5,27–29]
3. Decrease in the width of the G band at FWHM significant of less bond angle disorder [3,28,29]
4. Increase in size and/or number of aromatic domains (L_a) [30],
5. Increase in sp^2 content (or decrease in sp^3 content) [5,6,31,32]
6. Voids or porosity [6,33–36]Specific to this study:
7. The stress reduction achieved at 10 sccm nitrogen gas flow rate is less than at 20 sccm flow rate. (At 10 sccm flow, nitrogen makes up 11% of the total gas, and at 20 sccm the percentage of nitrogen in the total gas varies between 16–20%.)

8. The D peak becomes more pronounced with the addition of 20 sccm nitrogen and not at 10 sccm.

These observations can be interpreted according to three approaches. The first explanation can be made in terms of a chemical approach and the increase in the aromaticity of the carbon coating. The results show that addition of nitrogen at 20 sccm produces a more pronounced 'shoulder' or fitted D peak in the Raman spectra. The intensity of the fitted D peak relative to the G peak is increased, which is interpreted as an augmentation in aromatic rings. Since this observation is made with the addition of nitrogen at 20 sccm and not at 10 sccm, it is hypothesized that when nitrogen is present in the right proportion to the total gas feed $\sim 16\%$ or more, that it catalyses the development of aromatic ring structures. It can be envisioned that nitrogen once implanted into the Si base or the carbon network acts as nucleation points for the formation of aromatic structures. Concurrently, nitrogen can effectively end cap acetylenic linear species in the plasma [37], stabilizing them during impact. Nitrogen bonds to carbon in three ways CN, CN and CN. The first two types of bonds can be found in aromatic benzene type rings where the nitrogen has replaced a carbon atom. Increase in average cluster size with inclusion of nitrogen was also observed by Liu et al. [30]. Valentini et al. [29] suggest that while nitrogen incorporates in six membered rings, that it tends to break up large islands of aromatic domains by the formation of terminating NH bonds, thereby reducing the average coordination number or degree of crosslinking. Due to the greater electronegativity of nitrogen, the NH bond is stronger than the CH bond, therefore leading to the formation of more numerous but smaller aromatic domains. This also means that the average coordination number and hence the degree of crosslinking is reduced which leads to a less strained structure and lower values of elastic modulus. One can then use the two-phase model of Robertson [38] for a-C:H to account for the observations noted with the inclusion of nitrogen. In this model, π bonded clusters are dispersed in a second phase made up of a majority sp^3 bonded phase which may be either highly cross linked as in hard forms of a-C:H or mainly CH_2 groups as in softer more polymeric forms. It is the π bonded cluster phase that is influenced by the addition of nitrogen, and observations 1–5 and 8 (which is specific to this study) can be accounted for using this approach.

The second explanation and widely accepted theory for decrease in the intrinsic stress is through reduction in the mean coordination number of the atoms comprising the network by replacing carbon with nitrogen in the sp^3 region (second phase). As indicated before, one way that this can occur is for nitrogen to end cap acetylenic linear species in the plasma [37]. The analysis of Angus and Jansen [39], of a-C:H coatings, explains that films with hydrogen contents less than 37.5% will be 'overconstrained', as the coatings in this study contain less hydrogen than this critical amount, based solely on this criterion there should exist a high internal compressive stress. The constraint-counting model of Philips [40] and Thorpe [41] relates network rigidity to the mean network coordination number **r**.

$$\langle r \rangle = (4C_{sp^3} + 3C_{sp^2} - C_H)/(1 - C_H) \quad (3)$$

where C_{sp^3} is the carbon sp^3 content, C_{sp^2} is the carbon sp^2 content and C_H the hydrogen content in the a-C:H(N) films [6]. As nitrogen has a coordination number of three, replacing carbon with nitrogen implies reduction in the average co-ordination number [4,6,29,30,36,38,42–44] of the sp^3 region, which will also lead to lower distortion of sp^2 clusters. Intrinsic stress, elastic modulus [24,45] and hardness are all reduced as the average coordination number is decreased. Atomic nitrogen, therefore acts as a network terminator and breaks up the structure. Assuming that at 10 sccm flow rate or when nitrogen makes up approximately 11% of the total gas composition, the reduction in the stress is solely due to a reduction in the coordination number, this theory helps explain observation #7.

The third explanation for stress reduction is that nitrogen addition causes an increase in density of voids [6]. In this study, the increase in open space (voids) observed with PBA occurs at the interface. In addition, this open space was not detected until annealing tests were started which indicates that the cavities were decorated with physisorbed hydrogen. This observation combined with the increase in aromatic clustering could indicate a non-uniform distribution of hydrogen [39], which may be associated with the interface of aromatic clusters. Reimer et al. [46] have used proton magnetic resonance to establish that hydrogen nuclei aggregate at carbon clusters in a-C:H, and that there may also be phase inhomogeniety where the rest of the amorphous carbon matrix is weakly hydrogenated. The existence of bound and unbound hydrogen in a-C films was shown by Nyaiesh and Nowak [47]. This hydrogen is verified to be associated with surfaces. They proposed that the film microstructure was permeable to hydrogen and interconnected by pores. It is conceivable that the open spaces detected in this study coalesce and become micro-cavities that are interconnected. These cavities may then be too big for detection with PBA and that is why they remained undetected with annealing. Other researchers have also noted a predilection for the formation of interconnected voids with nitrogen incorporation in the amorphous matrix [33–36]. Like the aromatic sp^2 clusters, the formation of voids also reduces strain [39]. A tensile stress is generated in films rich in voids [26], which means that the nitrogen containing sample showing greater open space at the interface experiences a lower interfacial stress. This effect may be confined to the interface, in which case it could indicate that the stress in the coating is graded, that is, it is less compressive at the Si/C interface than at the carbon/air interface. Although the net effect is still compressive the overall stress is reduced because of this. This theory explains observation six directly but as it can be associated

indirectly with aromatic clusters it collaborates observations 2–5.

The observations in this study can only be explained using a combination of three theories;, therefore, we propose that stress reduction with nitrogen inclusion is indeed achieved in different ways, which are not mutually exclusive. It can further be hypothesized that different process conditions may favor a particular stress reduction mechanism/s.

5. Conclusions

The results form this research show that in the modified PVD process, addition of nitrogen to the gas feed results in a reduction of the intrinsic stress in a-C:H coatings. The way in which this stress reduction is achieved is explained in terms of three theories: increased aromaticity of the coating, reduction in the coordination number of the network, and interfacial voids. It is seen that interpretation of all results is only possible when all theories are used. Therefore, it is shown that when nitrogen is present at 11% of the total gas flow, the reduction in intrinsic stress is achieved by substitution of nitrogen for carbon in the network. At 16% nitrogen inclusion, the formation of aromatic clustering is favored. Nitrogen doping also creates vacancy defects in the coating, and interfacial voids that are decorated with hydrogen and only detected after annealing between 150 and 400 °C.

Acknowledgements

This work is part of the research program of the 'Stichting voor Fundamenteel Onderzoek der Materie (FOM)', which is financially supported by the'Nederlandse Organisatie voor Wetenschappelijk Onderzoek (NWO)'. Appreciation is also extended to the Netherlands Institute of Metals Research (NIMR) and Delft University of Technology (TUDelft) for use of equipment and facilities. F. Rabbani would like to thank Prof. Schoonman for stimulating discussions regarding the work described.

References

[1] K. Chakrabarti, M. Basu, S. Chaudhuri, A.K. Pal, H. Hanzawa, Vacuum 53 (1999) 405–413.
[2] P. Wood, T. Wydeven, O. Tsuji, Thin Solid Films 258 (1995) 151–158.
[3] D.-J. Jan, C.-F. Ai, Mater. Chem. Phys. 72 (2001) 158–162.
[4] D.F. Franceschini, C.A. Achete, F.L. Freire, Appl. Phys. Lett. 60 (1992) 3229–3231.
[5] C. Lenardi, M.A. Baker, V. Briois, L. Nobili, P. Piseri, W. Gissler, Diamond Relat. Mater. 8 (1999) 595–600.
[6] Y.H. Cheng, Y.P. Wu, J.G. Chen, X.L. Qiao, C.S. Xie, Diamond Relat. Mater. 8 (1999) 1214–1219.
[7] D.F. Franceschini, F.L. Freire, S.R.P. Silva, Appl. Phys. Lett. 68 (1996) 2645–2647.
[8] A. van Veen, H. Schut, P.E. Mijnarends, in: P. Coleman (Ed.), Positron Beams and their Applications, World Scientific, Singapore, 1999, pp. 191–224.
[9] G. Leusink, Thesis: Growth and Properties of CVD-W films for Microelectronic Applications-A Study on Growth Related Stress, TU Delft, Delft, 1994, pp. 35–41.
[10] R.W. Hoffman, Physics of Thin Films, Academic, New York, 1966, p. 3.
[11] W.C. Oliver, G.M. Pharr, J Mater. Res. 7 (1992) 1564–1583.
[12] A.C. Ferrari, J. Robertson, Phys. Rev. B 61 (2000-II) 14095–14107.
[13] A. van Veen, J. Trace Microprobe Tech. 8 (1–2) (1990) 1–29.
[14] A. van Veen, H. Schut, J. de Vries, R.A Hakvoort, M.R. Ijpma, in: P.J. Massoumi, G.R. Massoumi, P.J. Simpson (Eds.), AIP 218, Positron Beams for Solids and Surfaces, American Institute of Physics, New York, 1991, pp. 171–196.
[15] W.M. Arnoldbik, F.H.P.M. Habraken, Rep. Prog. Phys. 56 (1993) 859–902.
[16] C.H.M.Marée,A.M.Vredenberg,F.H.P.M.Habraken,MatChemPhysPhys. Phys. 46 (1996) 198–205.
[17] E.T. Prince, M.M. Romach, J. Vac. Sci. Technol. A 3 (1985) 694–695.
[18] J. Schwan, S. Ulrich, V. Batori, H. Ehrhardt, S.R.P. Silva, J. Appl. Phys. 80 (1996) 440–447.
[19] A.J. Papworth, C.J. Kiely, A.P. Burden, S.R.P. Silva, G.A.J Amaratunga, Phys. Rev. B 62 (2000) 12628–12631.
[20] B. Dischler, A. Bubenzer, P. Koidl, Solid State Commun. 48 (1983) 105–108.
[21] J.C. Angus, P. Koidl, S. Domitz, in: J. Mort, F. Jansen (Eds.), Plasma Deposited Thin Films, CRC Press, Boca Raton, 1986, pp. 119–123.
[22] R.O. Dillon, J.A. Woollam, V. Katkanant, Phys. Rev. B 29 (1984) 3482–3489.
[23] A.V. Fedorov, A.van Veen, H. Schut, Mater. Sci. Forum 363–365 (2001) 646–648.
[24] M.M. de Lima, R.G. Lacerda, J. Vilcarromero, F.C. Marques, J. Appl. Phys. 86 (1999) 4936–4942.
[25] J.S.Wang,Y.Sugimura,A.G.Evans,W.K.Tredway,ThinSolidFilmsFilms Films 325 (1998) 163–174.
[26] F.C. Marques, J. Vilcarromero, R.G. Lacerda, Appl. Phys. A 71 (2000) 633–637.
[27] D.P. Magill, A.A. Ogwu, J.A. McLaughlin, P.D. Maguire, R.W. McCullough, D. Voulot, et al, J. Vac. Sci. Technol. A 19 (2001) 2462.
[28] G. Mariotto, F.L. Freire, C.A. Achete, Thin Solid Films 241 (1994) 255–259.
[29] L. Valentini, J.M. Kenny, G. Carlotti, M. Guerrieri, G. Signorelli, L. Lozzi, et al, Thin Solid Films 389 (2001) 315–320.
[30] Y. Liu, F. Demichelis, A. Tagliaferro, Solid State Commun. 100 (1996) 597–602.
[31] B.K. Yen, J.-U. Thiele, M. Geisler, P.H. Kasai, R.L. White, B.R. York, et al, IEEE Trans. Magn. 37 (2001) 1786–1788.
[32] B. Kleinsorge, A.C. Ferrari, J. Robertson, W.I Milne, S. Waidmann, S. Hearne, Diamond Relat. Mater. 9 (2000) 643–648.
[33] F.L. Freire, C.A. Achete, G. Mariotto, R. Canteri, J. Vac. Sci. Technol. A 12 (1994) 3048–3053.
[34] J. Schwan, W. Dworschak, K. Jung, H. Ehrhardt, Diamond Relat. Mater. 3 (1994) 1034–1039.
[35] D.F. Franceschini, C.A. Achete, F.L. Freire, W. Beyer, G. Mariotto, Diamond Relat. Mater. 3 (1993) 88–93.
[36] F.L. Freire, C.A. Achete, R.S. Brusa, G. Mariotto, T. Teng, A. Zecca, Solid State Commun. 91 (1994) 965–970.
[37] S. Yang, K.J. Taylor, M.J. Craycraft, J. Conceicao, C.L. Pettiette, O. Cheshnovsky, et al, Chem. Phys. Lett. 144 (1988) 431–436.
[38] J. Robertson, Phys. Rev. Lett. 68 (1992) 220–223.
[39] J.C. Angus, F. Jansen, J. Vac. Sci. Technol. A 6 (1988) 1778–1782.
[40] J.C. Philips, J. Non-Cryst. Solids 34 (1979) 153.
[41] M.F. Thorpe, J. Non-Cryst. Solids 182 (1995) 135–142.

[42] D. Franceschini, C. Achete, F. Freire, G. Mariotto, in: F. Demichelis, D. De Martino, C.F. Pirri, A. Tagliaferro (Eds.), Mat. Res. Soc. Symp. Proc. 270 (1992) 481–486.
[43] S. Zhang, H. Xie, X. Zeng, P. Hing, Surf. Coat. Technol. 122 (1999) 219–224.
[44] S.R.P Silva, J. Robertson, G.A.J. Amaratunga, B. Rafferty, L.M. Brown, J. Schwan, et al, J. Appl. Phys. 81 (1997) 2626–2634.
[45] S. Sattel, J. Robertson, H. Ehrhardt, J. Appl. Phys. 82 (1997) 4566–4576.
[46] J.A. Reimer, R.W. Vaughan, J.C. Knights, R.A. Lujan, J. Vac. Sci. Technol. 19 (1981) 53–56.
[47] A.R. Nyaiesh, W.B. Nowak, J. Vac. Sci. Technol. A 1 (1983) 308–312.